Nonlin. Processes Geophys. Discuss., 1, 519–541, 2014
www.nonlin-processes-geophys-discuss.net/1/519/2014/
doi:10.5194/npgd-1-519-2014

Nonlinear Processes in Geophysics
Discussions
Open Access

On the nonlinear feedback loop and energy cycle of the non-dissipative Lorenz model

B.-W. Shen

ESSIC, University of Maryland, College Park, Mesoscale Atmospheric Processes Laboratory, Code 612, NASA Goddard Space Flight Center, Greenbelt, MD 20771, USA

Received: 12 February 2014 – Accepted: 23 March 2014 – Published: 11 April 2014

Correspondence to: B.-W. Shen (bo-wen.shen-1@nasa.gov; bowen.shen@gmail.com)

Published by Copernicus Publications on behalf of the European Geosciences Union & American Geophysical Union.

Abstract

In this study, we discuss the role of the nonlinear terms and linear (heating) term in the energy cycle of the three-dimensional (X–Y–Z) non-dissipative Lorenz model (3D-NLM). (X, Y, Z) represent the solutions in the phase space. We first present the closed-form solution to the nonlinear equation $d^2X/d\tau^2 + (X^2/2)X = 0$, τ is a non-dimensional time, which was never documented in the literature. As the solution is oscillatory (wave-like) and the nonlinear term (X^2) is associated with the nonlinear feedback loop, it is suggested that the nonlinear feedback loop may act as a restoring force. We then show that the competing impact of nonlinear restoring force and linear (heating) force determines the partitions of the averaged available potential energy from Y and Z modes, respectively, denoted as $\overline{\text{APE}_Y}$ and $\overline{\text{APE}_Z}$. Based on the energy analysis, an energy cycle with four different regimes is identified with the following four points: $A(X, Y) = (0, 0)$, $B = (X_t, Y_t)$, $C = (X_m, Y_m)$, and $D = (X_t, -Y_t)$. Point A is a saddle point. The initial perturbation $(X, Y, Z) = (0, 1, 0)$ gives $(X_t, Y_t) = (\sqrt{2\sigma r}, r)$ and $(X_m, Y_m) = (2\sqrt{\sigma r}, 0)$. σ is the Prandtl number, and r is the normalized Rayleigh number. The energy cycle starts at (near) point A, $A^+ = (0, 0^+)$ to be specific, goes through B, C, and D, and returns back to A, i.e., $A^- = (0, 0^-)$. From point A to point B, denoted as Leg A–B, where the linear (heating) force dominates, the solution X grows gradually with $\{\overline{\text{KE}}\uparrow, \overline{\text{APE}_Y}\downarrow, \overline{\text{APE}_Z}\downarrow\}$. $\overline{\text{KE}}$ is the averaged kinetic energy. We use the upper arrow ($\uparrow$) and down arrow ($\downarrow$) to indicate an increase and decrease, respectively. In Leg B–C (or C–D) where nonlinear restoring force becomes dominant, the solution X increases (or decreases) rapidly with $\{\overline{\text{KE}}\uparrow, \overline{\text{APE}_Y}\uparrow, \overline{\text{APE}_Z}\downarrow\}$ (or $\{\overline{\text{KE}}\downarrow, \overline{\text{APE}_Y}\downarrow, \overline{\text{APE}_Z}\uparrow\}$). In Leg D–A, the solution X decreases slowly with $\{\overline{\text{KE}}\downarrow, \overline{\text{APE}_Y}\uparrow, \overline{\text{APE}_Z}\uparrow\}$. As point A is a saddle point, the aforementioned cycle may be only half of a "big" cycle, displaying the wing pattern of a glasswinged butterfly, and the other half cycle is antisymmetric with respect to the origin, namely $B = (-X_t, -Y_t)$, $C = (-X_m, 0)$, and $D = (-X_t, Y_t)$.

NPGD
1, 519–541, 2014

1 Introduction

It has been fifty years since Lorenz published his breakthrough modeling study (Lorenz, 1963) which has changed the view on the predictability of weather and climate (Solomon et al., 2007) and later laid the foundation for chaos theory (e.g., Gleick, 1987; Anthes, 2011). His model with three Fourier modes, which represent the solution to the 2-D Rayleigh–Benard equation (Saltzman, 1962; Lorenz, 1963), is referred to as the three-dimensional Lorenz model (3DLM). We use 3D-NLM to refer to as the non-dissipative version which will be introduced later. It is now accepted that weather is chaotic with a finite predictability and that the source of chaos is nonlinearity. As the degree of nonlinearity is finite in the 3DLM, the impact of increased nonlinearity on systems' solutions and/or their stability has been studied using the generalized LMs with additional Fourier modes (e.g., Curry, 1978; Curry et al., 1984; Howard and Krishnamurti, 1986; Hermiz et al., 1995; Thiffeault and Horton, 1996; Musielak et al., 2005; Roy and Musielak, 2007a). As compared to the 3DLM, some of the generalized LMs suggested larger Rayleigh number values (or heating parameters) for the onset of chaos, while the other showed smaller values. This discrepancy may be attributed to different mode truncations (e.g., Curry et al., 1984; Thiffeault and Horton, 1996; Roy and Musielak, 2007a, b, c; Shen, 2014a, b) that lead to the different degree of nonlinearity and different systems whose energy may be or may not be conserved (e.g., Roy and Musielak, 2007a). Among the studies with the generalized LMs, the pioneering study of Prof. Curry (Curry et al., 1984) suggested that chaotic responses disappeared when sufficient modes were included. Recent studies by Prof. Musielak and his colleagues (Musielak et al., 2005; Roy and Musielak, 2007a, b, c) examined the transition to chaos and fractal dimensions of generalized LMs, and emphasized the importance of proper mode truncation in the energy conservation. A more recent study (Shen, 2014a) discussed the importance of proper Fourier mode selection in extending the nonlinear feedback loop of the 3DLM. The feedback loop is defined as a pair of downscale and upscale transfer processes associated with the Jacobian

NPGD
1, 519–541, 2014

function (in Eq. 2). It was suggested that the original feedback loop may help stabilize the solution for $1 < r < 24.74$ in the 3DLM and that the extended nonlinear feedback loop in a five-dimensional LM (5DLM) can provide negative nonlinear feedback to produce non-trivial stable critical points when $1 < r < 43.5$. It was then hypothesized that a system's stability can be improved further with more modes that can provide negative nonlinear feedback. While the impact of the increased degree of nonlinearity with more Fourier modes is important and studies are being conducted, the competing role of the nonlinear terms with the linear (heating) term and/or dissipative terms deserves to be examined to understand the conditions under which the nonlinear processes may lead to stable or chaotic solutions.

It has been shown (e.g., Roupas, 2012) that the 3DLM in the dissipative limit, which is referred to as the 3D-NLM, contains two conserved quantities that represent the conservation of $(\overline{KE} + \overline{PE})$ and $(\overline{KE} + \overline{APE})$, respectively. Here, $\overline{KE}$, $\overline{PE}$, and $\overline{APE}$ are the domain-averaged kinetic energy, potential energy and available potential energy, respectively. These two quantities are related to the Nambu Hamiltonians. (Nambu, 1973; Nevir and Blender, 1994; Floratos, 2011; Roupas, 2012; Blender and Lucarini, 2013). As a result of the conservation properties, the collective impact of the nonlinear feedback loop and linear (heating) term may effectively act as a "restoring" force. The simplicity of the 3D-NLM enables us to examine how the nonlinear feedback loop and linear (heating) term work together to produce oscillatory solutions (in the phase space). This will be addressed in conjunction with how the available potential energy are partitioned among two different Fourier modes, one of which (Z) is included to enable the nonlinear feedback loop.

The paper is organized as follows. In Sect. 2, we present the governing equations and the 3D-NLM, introduce the nonlinear feedback loop, and derive the energy conservation laws. In Sect. 3, we illustrate the role of nonlinear terms in playing a restoring force and present an energy cycle with four regimes based on the tendency of $\overline{KE}$ and the partition of $\overline{APE}$ at different scales. Concluding remarks are given near the end.

NPGD
1, 519–541, 2014

2 Governing equations and the non-dissipative Lorenz model

The following governing equations for a 2D (x,z), Boussinesq flow are introduced to derive the non-dissipative Lorenz model (3D-NLM) and calculate its kinetic and potential energy

$$\frac{\partial}{\partial t}\nabla^2\psi = -J(\psi,\nabla^2\psi) + g\alpha\frac{\partial\theta}{\partial x} + \cancel{\nu\nabla^4\psi}, \tag{1}$$

$$\frac{\partial\theta}{\partial t} = -J(\psi,\theta) + \frac{\Delta T}{H}\frac{\partial\psi}{\partial x} + \cancel{\kappa\nabla^2\theta}, \tag{2}$$

where ψ is the streamfunction that gives the $u = -\psi_z$ and $w = \psi_x$, which represent the horizontal and vertical velocity perturbations, respectively, and θ is the temperature perturbation. ΔT represents the temperature difference at the bottom and top boundaries. The constants, g, α, ν, and κ denote the acceleration of gravity, the coefficient of thermal expansion, the kinematic viscosity, and the thermal diffusivity, respectively. The Jacobian of two arbitrary functions is defined as $J(A,B) = (\partial A/\partial x)(\partial B/\partial z) - (\partial A/\partial z)(\partial B/\partial x)$. The crossout symbol indicates the negligence of a term in the dissipationless limit. Equations (1) and (2) with the dissipative terms were first used in Saltzman (1962) and Lorenz (1963).

The non-dissipative Lorenz model (3D-NLM) is written as:

$$\frac{\mathrm{d}X}{\mathrm{d}\tau} = \sigma Y, \tag{3}$$

$$\frac{\mathrm{d}Y}{\mathrm{d}\tau} = -XZ + rX, \tag{4}$$

$$\frac{\mathrm{d}Z}{\mathrm{d}\tau} = XY. \tag{5}$$

Here (X,Y,Z) represent the amplitude of the Fourier modes. $\tau = \kappa(1+a^2)(\pi/H)^2 t$ is the dimensionless time. a is a ratio of the vertical scale of the convection cell to

NPGD
1, 519–541, 2014

its horizontal scale. H is the domain height, and $2H/a$ represents the domain width. $\sigma = \nu/\kappa$ (the Prandtl number), and $r = R_a/R_c$ (the normalized Rayleigh number, or the heating parameter). R_a is the Rayleigh number, $R_a = g\alpha H^3 \Delta T/\nu\kappa$ and R_c is its critical value for the free-slip Rayleigh–Benard problem, $R_c = \pi^4(1+a^2)^3/a^2$. The "forcing" terms on the right-hand side of Eqs. (4) and (5) are referred to as a linear force or heating term (rX) and nonlinear force terms ($-XZ$ and XY).

The 3D-NLM is integrated forward in time with the Runge–Kutta scheme. Without loss of generality, we only chose two different values of the normalized Rayleigh number r ($r = 25$, and $r = 45$) with other parameters kept as constant, including $\sigma = 10$ and $a = 1/\sqrt{2}$. A dimensionless time interval ($\Delta\tau$) of 0.01 is used, and a total number of time steps is 10 000, giving a total dimensionless time (τ) of 100. A smaller τ is used to improve accuracy in Figs. 1 and 2. Initial conditions are given as

$$(X, Y, Z) = (0, 1, 0). \tag{6}$$

These settings were used to examine the stability of the 5DLM in Shen (2014a, b) which also discussed the dependence of solution on different r and σ.

2.1 The nonlinear feedback loop and energy conservation laws

It has been shown that the nonlinear terms in the 3D-NLM (and 3DLM) are from the Jacobian term $J(\psi, \theta)$ in Eq. (2). The nonlinear interaction of two wave modes via the Jacobian term can generate or impact a third wave mode through a downscale (or upscale) transfer process; its subsequent upscale (or downscale) transfer process can provide feedback to the incipient wave mode(s). It was illustrated (Shen, 2014a) that XY and $-XZ$ represent the downscale and upscale transfer processes, respectively, forming a nonlinear feedback loop. The feedback loop can be extended as new modes are properly included. In the following, we discuss the role of the nonlinear feedback loop of the 3D-NLM in the energy conservations and partition of available potential energy, which in turn help produce oscillatory solutions.

NPGD
1, 519–541, 2014

The domain-averaged kinetic energy ($\overline{\mathrm{KE}}$), potential energy ($\overline{\mathrm{PE}}$), and available potential energy ($\overline{\mathrm{APE}}$) are defined as follows (e.g., Thiffeault and Horton, 1996; Blender and Lucarini, 2013; Shen, 2014a, b):

$$\overline{\mathrm{KE}} = \frac{1}{2}\int_0^{2H/a}\int_0^{H}(u^2+w^2)\mathrm{d}z\mathrm{d}x, \tag{7}$$

$$\overline{\mathrm{PE}} = -\int_0^{2H/a}\int_0^{H}g\alpha(z\theta)\mathrm{d}z\mathrm{d}x, \tag{8}$$

$$\overline{\mathrm{APE}} = -\frac{g\alpha H}{2\Delta T}\int_0^{2H/a}\int_0^{H}(\theta)^2\mathrm{d}z\mathrm{d}x. \tag{9}$$

Through straightforward derivations, we obtain the following:

$$\overline{\mathrm{KE}} = \frac{C_o}{2}X^2, \tag{10}$$

$$\overline{\mathrm{PE}} = -C_o\sigma Z, \tag{11}$$

$$\overline{\mathrm{APE}} = -\frac{C_o}{2}\frac{\sigma}{r}(Y^2+Z^2), \tag{12}$$

here $C_o = \pi^2\kappa^2\left(\frac{1+a^2}{a}\right)^3$. $\overline{\mathrm{APE}}$ is non-negative, as any perturbation reduces the energy transformable to $\overline{\mathrm{KE}}$.

Equations (10) and (11) lead to

$$\overline{\mathrm{KE}} + \overline{\mathrm{PE}} = C_o\left(\frac{X^2}{2} - \sigma Z\right) = C_1, \tag{13}$$

NPGD
1, 519–541, 2014

while Eqs. (10) and (12) give

$$\overline{\mathrm{KE}} + \overline{\mathrm{APE}} = \frac{C_o}{2}\left(X^2 - \frac{\sigma}{r}(Y^2 + Z^2)\right) = C_2. \tag{14}$$

With Eqs. (3)–(5), the time derivative of both Eqs. (13) and (14) is zero, so these two equations present the energy conservations. Both C_1 and C_2 are constants and are determined by the initial conditions. Thus, if we express Z and Y^2 as functions of X, they are single valued. To facilitate our discussions, the contribution to the APE from an individual mode is defined as $\overline{\mathrm{APE}_I} = -C_o \sigma I^2/2r$, here $I = Y$ or Z. Therefore, $\overline{\mathrm{APE}} = \overline{\mathrm{APE}_Y} + \overline{\mathrm{APE}_Z}$. Note that Eqs. (13) and (14) are related to the two Nambu Hamiltonians, $C = -X^2/2 + \sigma Z$ and $H = Y^2/2 + Z^2/2 - rZ$ (Nambu, 1973; Nevir and Blender, 1994; Floratos, 2011; Roupas, 2012; Blender and Lucarini, 2013).

From the initial conditions in Eq. (6), we have $C_1 = 0$ and $C_2/C_o = -\sigma/2r$, the latter of which is -0.2 for $r = 25$ and -0.11 for $r = 45$. Figure 1 shows the time evolution of the conserved quantities: $(\overline{\mathrm{KE}} + \overline{\mathrm{PE}})$ and $(\overline{\mathrm{KE}} + \overline{\mathrm{APE}})$ in Eqs. (13) and (14) from the 3D-NLM. At a larger r (e.g., $r = 45$), a finer $\Delta\tau$ is required to improve the numerical accuracy of simulated total energy (Fig. 1c). In this study, unless stated otherwise, C_1 and C_2 are assumed to be zero.

3 Discussions

In this section, we discuss the competing role of the nonlinear terms and the linear forcing term in the transient solutions and the energy cycle of the the 3D-NLM. From Eqs. (3), (4), and (13), we obtain

$$\frac{\mathrm{d}^2 X}{\mathrm{d}\tau^2} + M^2 X = 0, \tag{15a}$$

NPGD
1, 519–541, 2014

and

$$M^2 = \frac{X^2}{2} - \left(\sigma r + \frac{C_1}{C_o}\right). \tag{15b}$$

The three terms on the right-hand side of Eq. (15b) represent the impact of nonlinearity, linear (heating) force and initial conditions, respectively. Their competing impact (i.e., their differences) determines the sign of M^2, and thus the characteristics of the solution. Based on the relative magnitude of the initial state which may lead to $(\sigma r + C_1/C_o) \le 0$ or > 0, two types of solutions can be identified (Roupas, 2012). The characteristics of the two-type solutions are discussed using the selected ICs, giving $C_1 = 0$, in Sects. 3.2 and 3.3, respectively. To understand the role of the nonlinear terms (i.e., the nonlinear feedback loop), we begin our discussions with solving the solution to the equation with no nonlinear terms.

3.1 Linear solutions with $M^2 = -\sigma r$

Assuming no nonlinear terms in the 3D-NLM, we have two equations: $\mathrm{d}X/\mathrm{d}\tau = \sigma Y$ and $\mathrm{d}Y/\mathrm{d}\tau = rX$ and only one conservation law, as follows:

$$\overline{\mathrm{KE}} + \overline{\mathrm{APE}} = \frac{C_o}{2}\left(X^2 - \frac{\sigma}{r}Y^2\right) = C_2. \tag{16}$$

This linear case gives $M^2 = -\sigma r$, and Eq. (15) becomes $\mathrm{d}^2X/\mathrm{d}\tau^2 - \sigma r X = 0$. Therefore, the solution is

$$X = X_1 e^{-\sqrt{\sigma r}\tau} + X_2 e^{+\sqrt{\sigma r}\tau}, \tag{17}$$

here, X_1 and X_2 are constant coefficients. The origin, $(X, Y) = (0, 0)$, is a saddle point, and the trajectory is hyperbolic with solutions exhibiting exponential growth and decay. The initial condition, which determines $\mathrm{d}X/\mathrm{d}Y$ $(= \sigma Y/rX)$, can help select

NPGD
1, 519–541, 2014

the proper mode(s). For example, $(X,Y)=(\sqrt{\sigma/r},1)$ only gives the growing mode with $(X_1,X_2)=(0,\sqrt{\sigma/r})$, while $(X,Y)=(\sqrt{\sigma/r},-1)$ leads to the decaying mode with $(X_1,X_2)=(\sqrt{\sigma/r},0)$. The former and latter show the properties of the unstable and stable manifolds, respectively (Ide et al., 2002). In the nonlinear case, a "current" state may vary with time, so either mode may appear at different stages, as shown in Sect. 3.3. Based on Eqs. (16) and (17), although the time change of $(\overline{\mathrm{KE}}+\overline{\mathrm{APE}})$ remains zero, the $\overline{\mathrm{KE}}$ produced with only the linear (heating) force has no upper limit. This could violate the linear assumption, and thus nonlinearity should be included.

3.2 Nonlinear solutions with $M^2 = X^2/2$ and nonlinear restoring force

Here, we consider a special case with $r=0$, leading to $M^2=X^2/2$. Thus, Eq. (15) becomes

$$\frac{\mathrm{d}^2X}{\mathrm{d}\tau^2}+\frac{X^2}{2}X=0. \tag{18}$$

As compared to the case with $r\neq 0$ in Eqs. (13) and (14), the energy conservation laws with $r=0$ are:

$$\frac{X^2}{2}-\sigma Z=0, \tag{19}$$

$$Y^2+Z^2=1, \tag{20}$$

which in turn leads to

$$Y^2+\frac{X^4}{4\sigma^2}=1. \tag{21}$$

NPGD
1, 519–541, 2014

The solutions to the above equation are:

$$X^2 = 2\sigma\sin(\phi), \tag{22a}$$

$$Y = \cos(\phi), \tag{22b}$$

$$Z = \sin(\phi), \tag{22c}$$

where the phase function ϕ can be determined from Eqs. (18) and (22a) and is written as

$$\phi = \int_0^\tau X \mathrm{d}\tau_o, \tag{23a}$$

which can be also displayed as

$$\phi = \int_0^\tau \int_0^\tau \sigma Y \mathrm{d}\tau_1 \mathrm{d}\tau_2. \tag{23b}$$

To illustrate the solution's characteristics, Eqs. (22b) and (23b) are solved using the following iterated method:

$$Y_n = \cos(\phi_n), \quad n = 0, 1, 2 \ldots N \tag{24a}$$

$$\phi_{n+1} = \int_0^\tau \int_0^\tau \sigma Y_n \mathrm{d}\tau_1 \mathrm{d}\tau_2, \tag{24b}$$

here N is the number of iterations. During a period of time, an initial guess for the phase function is given as $\phi_0(\tau) = \tau$. We insert the first phase function ϕ_0 into Eq. (24a) to obtain Y_0, and then calculate the next phase function ϕ_1 using Y_0 and Eq. (24b). The integral of Eq. (24b) is calculated using the trapezoidal rule. We then repeat the

NPGD
1, 519–541, 2014

above calculations for N times. Numerical results with $N = 100$ are shown in Fig. 2. The phase function oscillates with time and varies between 0 and π, which is consistent with Eq. (22a) as a result of $\sin(\phi) \geq 0$. Therefore, the solution to Eq. (18) is oscillatory instead of growing or decaying exponentially (shown in Fig. 2b and c). It is suggested that the nonlinear term in Eq. (18) may be viewed as a nonlinear restoring force. This is consistent with the view (Shen, 2014a) that the pair of the nonlinear terms ($-XZ$ and XY), leading to the nonlinear term ($X^2/2$), can form a nonlinear feedback loop in the 3DLM. As a result of the simple method for the integral calculation, a fine $\Delta\tau$ may be required to obtain accurate resolutions. This is shown by the red and green lines for the results with $\Delta\tau = 0.0001$ and 0.01, respectively (see Fig. 2a).

To verify the integral form of the solutions in Eq. (24a) and (24b), the numerical solutions of the 3D-NLM with $r = 0$ (e.g., Eqs. 3–5) are shown in Fig. 3. In panel (a), the blue "dot" shows the initial temporal evolution of the phase function that is calculated by performing time integration of X using Eq. (23a) where X is from the 3D-NLM, while the red line shows the phase function calculated with Eq. (24a) and (24b). They are in good agreement. The simulated trajectories in the X–Y and X–Z sections are elliptic and parabolic (Fig. 3b and c), respectively, which are consistent with the analytical relations in Eqs. (21) and (19), respectively. Figure 3d shows the time evolution of oscillatory Y (red) and X (blue), which are consistent with the results in Fig. 2b and c, respectively.

3.3 Nonlinear solutions with $M^2 = X^2/2 - \sigma r$ and an energy cycle

In the previous sections, we have illustrated the individual impact of the linear (heating) force and nonlinear feedback loop using the cases with $M^2 < 0$ and $M^2 \geq 0$, respectively, neither of which change the sign during the integration. Here, we consider the general case with $M^2 = (X^2/2 - \sigma r)$, whose sign may vary during the time integration, depending on the relative magnitude of the nonlinearity and the linear (heating) force. M^2 has two zeros at $X = \pm X_t$ and $X_t = \sqrt{2\sigma r}$, which are called turning points. Based on the analysis with the WKB approximation (Bender and Orszag, 1978),

NPGD
1, 519–541, 2014

there appears to be a growing or decaying solution for $|X| < X_t$ and an oscillatory (wave-like) solution for $|X| > X_t$. The former is impacted largely by the linear (heating) force while the latter by the nonlinear restoring force. Additional analyses are given below.

Equations (13) and (14) with $C_2 \approx 0$ gives:

$$Y^2 = \frac{1}{\sigma^2}\left(\sigma r X^2 - \frac{X^4}{4}\right). \quad (25)$$

$Y^2 \geq 0$ leads to $|X| \leq 2\sqrt{\sigma r}$, which gives a maximum of X ($X_{max} = 2\sqrt{\sigma r}$). Taking the partial derivative of Eq. (25) with respect to X tells us that Y has extrema when $X = \pm\sqrt{2\sigma r} = \pm X_t$. At $X = \pm X_t$, we observe $Z = r$ and $Y = \pm r$ from Eqs. (13) and (14), respectively, and thus $\overline{APE_Y} = \overline{APE_Z}$, namely equal contributions to $\overline{APE}$ from Y and Z modes. Furthermore, Eq. (25) suggests that Y^2 increases initially in association with the increase of X^2 but later decreases in association with the increase of X^4. The former is consistent with the linear case in Eq. (16), while the latter is consistent with the simplified nonlinear case in Eqs. (19) and (20). The distribution of Y as a function of X (i.e., Eq. 25) with the aforementioned four points is shown in Fig. 4. The energy cycle starts at point A, goes through B, C, and D, and returns back to A. The segment from point P to point Q is denoted as Leg P–Q, here P and Q are either one of the following: $A(X,Y) = (0,0)$, $B = (X_t, Y_t)$, $C = (X_m, Y_m)$, and $D = (X_t, -Y_t)$. Point A is a saddle point as discussed in Sect. 3.1. The initial perturbation $(X,Y,Z) = (0,1,0)$ gives $(X_t, Y_t) = (\sqrt{2\sigma r}, r)$ and $(X_m, Y_m) = (2\sqrt{\sigma r}, 0)$. The analysis is then inter-compared with the numerical results of the 3D-NLM below.

With the selected ICs, Fig. 5a shows the big cycle with two "small cycles" that are anti-symmetric with respect to the saddle point A. The big cycle resembles the wing of a glasswinged butterfly. The right-hand side wing shares the same characteristics as the cycle in Fig. 4, while the left-hand side wing is antisymmetric with respect to the origin. While the trajectories in X–Y are shown in Fig. 5a, the distribution of the $\overline{APE_Y}$ and $\overline{APE_Z}$ as a function of X is shown in Fig. 5c. From the perspective of the APE

NPGD
1, 519–541, 2014

partition, the $\overline{\mathrm{APE}_Y}$ (red) dominates in Leg *A*–*B* (*D*–*A*) while $\overline{\mathrm{APE}_Z}$ dominates in Leg *B*–*C* (*C*–*B*) where nonlinearity is stronger. Alternatively, $\overline{\mathrm{KE}}$ is converted predominantly from $\overline{\mathrm{APE}_Y}$ when X^2 is small, and it is mainly converted from $\overline{\mathrm{APE}_Z}$ when X^2 is large. Therefore, the inclusion of *Z* mode can lead to the oscillatory solution by enabling the partition of APE on different scales at different stages (i.e., linear and nonlinear stages).

Figure 6 shows time evolution of $\overline{\mathrm{APE}_Y}$ and $\overline{\mathrm{APE}_Z}$. The energy cycle starts at (near) point *A*, $A^+ = (0, 0^+)$ to be specific, goes through *B*, *C*, and *D*, and returns back to *A*, i.e., $A^- = (0, 0^-)$. In Leg *A*–*B*, where the linear (heating) force dominates, the solution *X* grows gradually with $\{\overline{\mathrm{KE}}\uparrow, \overline{\mathrm{APE}_Y}\downarrow, \overline{\mathrm{APE}_Z}\downarrow\}$ and $|\overline{\mathrm{APE}_Y}| > |\overline{\mathrm{APE}_Z}|$. In Leg *B*–*C* (or *C*–*D*) where nonlinear restoring force becomes dominant, the solution *X* increases (or decreases) rapidly with $\{\overline{\mathrm{KE}}\uparrow, \overline{\mathrm{APE}_Y}\uparrow, \overline{\mathrm{APE}_Z}\downarrow\}$ (or $\{\overline{\mathrm{KE}}\downarrow, \overline{\mathrm{APE}_Y}\downarrow, \overline{\mathrm{APE}_Z}\uparrow\}$) and $|\overline{\mathrm{APE}_Y}| < |\overline{\mathrm{APE}_Z}|$. In Leg *D*–*A*, the solution *X* decays slowly with $\{\overline{\mathrm{KE}}\downarrow, \overline{\mathrm{APE}_Y}\uparrow, \overline{\mathrm{APE}_Z}\uparrow\}$ and $|\overline{\mathrm{APE}_Y}| > |\overline{\mathrm{APE}_Z}|$. After the trajectory returns back to point A^-, it may experience another small cycle, going to B^-, C^-, and D^-, and returning back to point A^+. Here, $B^- = (-X_\mathrm{t}, -Y_\mathrm{t})$, $C^- = (-X_\mathrm{m}, Y_\mathrm{m})$, and $D^- = (-X_\mathrm{t}, Y_\mathrm{t})$. The two "small cycles" form the big cycle, which resembles the wing of a glasswinged butterfly, and the time evolution of energy is the same for both wings.

4 Concluding remarks

Over 50 years ago, Lorenz showed that chaos may appear in the presence of nonlinearity using the forced, dissipative Lorenz mode, suggesting that nonlinearity may be the source of chaos. In this study, we discussed how nonlinearity may act as a restoring force to produce oscillatory solutions using the non-dissipative Lorenz model (3D-NLM). We first presented the closed-form solution of the nonlinear equation $d^2X/d\tau^2 + (X^2/2)X = 0$, which is derived from the 3D-NLM with $r = 0$. The corresponding solution is oscillatory (wave-like) and the nonlinear term (X^2) is associated with the nonlinear feedback loop. Therefore, it is suggested that the

NPGD
1, 519–541, 2014

nonlinear feedback loop may act as a restoring force. To our best knowledge, these (i.e., the closed-form solution) have not been documented in the literature. Compared to the linear system, the inclusion of Z mode in the 3D-NLM not only introduces more APE to be transferred to KE but also limits KE to be finite. We illustrated that the relative impact of nonlinear restoring force and linear (heating) force determines the partitions of the averaged available potential energy associated with the Y and Z modes, respectively. Based on the energy analysis, an energy cycle with four different regimes is identified with the following four points: $A(X,Y) = (0,0)$, $B = (X_t, Y_t)$, $C = (X_m, Y_m)$, and $D = (X_t, -Y_t)$. With the initial perturbation $(X,Y,Z) = (0,1,0)$, we have $(X_t, Y_t) = (\sqrt{2\sigma r}, r)$ and $(X_m, Y_m) = (2\sqrt{\sigma r}, 0)$. The energy cycle may start at (near) point A, goes through B, C, and D, and returns back to A. As point A is a saddle point, the "cycle" is only half of the big cycle, which resembles the wing of the glasswinged butterfly. A summary on the energy cycle and the big cycle is given near the end of Sect. 3. The dependence of solutions on initial perturbations (i.e., Hamiltonian chaos) in the conservative 3D-NLM is being examined, and will be compared to that in the 3DLM to understand the role of the dissipative terms in solutions' stability.

Acknowledgements. We are grateful for support from the NASA Advanced Information System Technology (AIST) program of the Earth Science Technology Office (ESTO) and from the NASA Computational Modeling Algorithms and Cyberinfrastructure (CMAC) program. We would like to thanks Xubin Zeng for valuable discussions and Jill Dunbar for proofreading this manuscript. Resources supporting this work were provided by the NASA High-End Computing (HEC) Program through the NASA Advanced Supercomputing (NAS) Division at Ames Research Center.

References

Anthes, R.: Turning the tables on chaos: is the atmosphere more predictable than we assume?, UCAR Magazine, spring/summer, available at: https://www2.ucar.edu/atmosnews/opinion/turning-tables-chaos-atmosphere-more-predictable-we-assume-0 (last access: 6 May 2011), 2011. 521

NPGD
1, 519–541, 2014

Bender, C. M. and Orszag, S. A.: Advanced Mathematical Methods for Scientists and Engineers, McGraw-Hill, New York, 593 pp., 1978. 530
Blender, R. and Lucarini, V.: Nambu representation of an extended Lorenz model with viscous heating, Physica D, 243, 86–91, 2013. 522, 525, 526
Curry, J. H.: Generalized Lorenz systems, Commun. Math. Phys., 60, 193–204, 1978. 521
Curry, J. H., Herring, J. R., Loncaric, J., and Orszag, S. A.: Order and disorder in two- and three-dimensional Benard convection, J. Fluid Mech., 147, 1–38, 1984. 521
Floratos, E.: Matrix quantization of turbulence, Int. J. Bifurcat. Chaos, 22, 1250213, doi:10.1142/S0218127412502136, 2012. 522, 526
Gleick, J.: Chaos: Making a New Science, Penguin, New York, 360 pp., 1987. 521
Hermiz, K. B., Guzdar, P. N., and Finn, J. M.: Improved low-order model for shear flow driven by Rayleigh–Benard convection, Phys. Rev. E, 51, 325–331, 1995. 521
Howard, L. N. and Krishnamurti, R. K.: Large-scale flow in turbulent convection: a mathematical model, J. Fluid Mech, 170, 385–410, 1986. 521
Lorenz, E.: Deterministic nonperiodic flow, J. Atmos. Sci., 20, 130–141, 1963. 521, 523
Ide, K., Small, D., and Wiggins, S.: Distinguished hyperbolic trajectories in time-dependent fluid flows: analytical and computational approach for velocity fields defined as data sets, Nonlin. Processes Geophys., 9, 237–263, doi:10.5194/npg-9-237-2002, 2002. 528
Solomon, S., Qin, D., Manning, M., Chen, Z., Marquis, M., Averyt, K., Tignor, M., and Miller Jr., H. L. (Eds.): Climate Change 2007: The Physical Science Basis, Cambridge University Press, 996 pp., 2007. 521
Musielak, Z. E., Musielak, D. E. and Kennamer, K. S.: The onset of chaos in nonlinear dynamical systems determined with a new fractal technique, Fractals, 13, 19–31, 2005. 521
Nambu, Y.: Generalized Hamiltonian dynamics, Phys. Rev. D, 7, 2403, doi:10.1103/PhysRevD.7.2405, 1973. 522, 526
Nevir, P. and Blender, R.: Hamiltonian and Nambu representation of the non-dissipative Lorenz equations, Beitraege zur Physik der Atmosphaere, 67, 133–140, 1994. 522, 526
Roupas, Z.: Phase space geometry and chaotic attractors in dissipative nambu mechanics, J. Phys. A-Math. Theor., 45, 195101, doi:10.1088/1751-8113/45/19/195101, 2012. 522, 526, 527
Roy, D. and Musielak, Z. E.: Generalized Lorenz models and their routes to chaos. I. energy-conserving vertical mode truncations, Chaos Soliton. Fract., 32, 1038–1052, 2007a. 521

NPGD
1, 519–541, 2014

Roy, D. and Musielak, Z. E.: Generalized Lorenz models and their routes to chaos. II. Energy-conserving horizontal mode truncations, Chaos Soliton. Fract., 31, 747–756, 2007b. 521
Roy, D. and Musielak, Z. E.: Generalized Lorenz models and their routes to chaos. III. Energy-conserving horizontal and vertical mode truncations, Chaos, Solitons and Fractals, 33, 1064–1070, 2007c. 521
Saltzman, B.: Finite amplitude free convection as an initial value problem, J. Atmos. Sci., 19, 329–341, 1962. 521, 523
Shen, B.-W.: Nonlinear feedback in a five-dimensional Lorenz model, J. Atmos. Sci., doi:10.1175/JAS-D-13-0223.1, in press, 2014a. 521, 524, 525, 530
Shen, B.-W.: Nonlinear Feedback in a Six-dimensional Lorenz Model: Impact of an Additional Heating Term, J. Atmos. Sci., submitted, 2014b. 521, 524, 525, 536
Thiffeault, J.-L. and Horton, W.: Energy-conserving truncations for convection with shear flow, Phys. Fluids, 8, 1715–1719, 1996. 521, 525

NPGD
1, 519–541, 2014

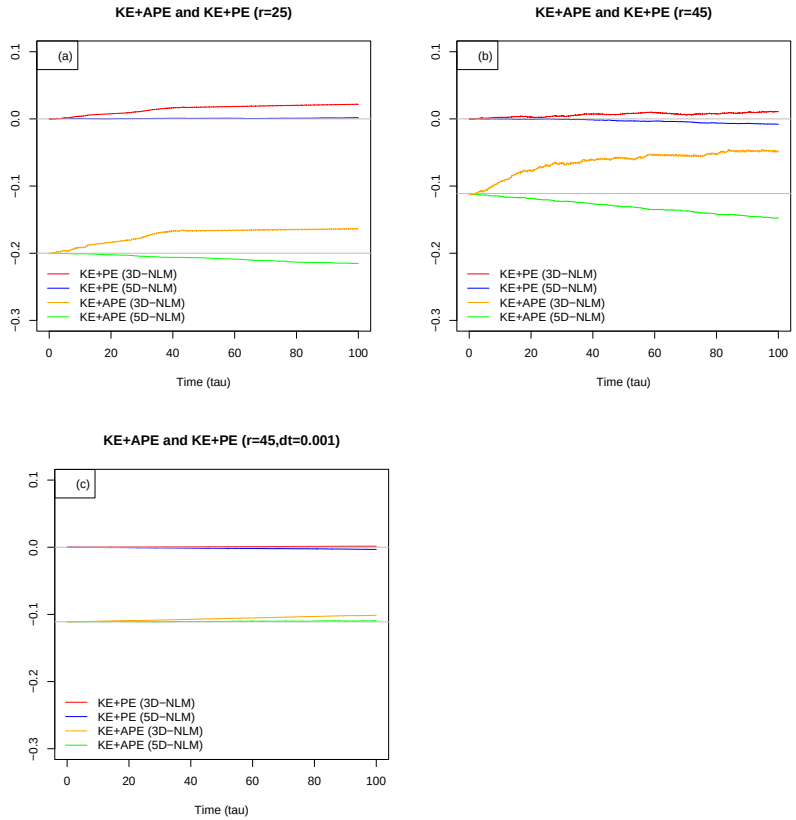

Fig. 1. Time evolution of (KE + PE) and (KE + APE) from the 3D-NLM and 5D-NLM (Shen, 2014b). Panels **(a)** and **(b)** are for $r = 25$, and $r = 45$, respectively. Results from the 5D-NLM are presented to show the dependence of (spatial) resolutions. In comparison, **(c)** shows the dependence of the temporal resolution with $\Delta\tau = 0.0001$. All fields are normalized by the constant $C_o \left(= \pi^2 \kappa^2 \left(\frac{1+a^2}{a} \right)^3 \right)$.

NPGD
1, 519–541, 2014

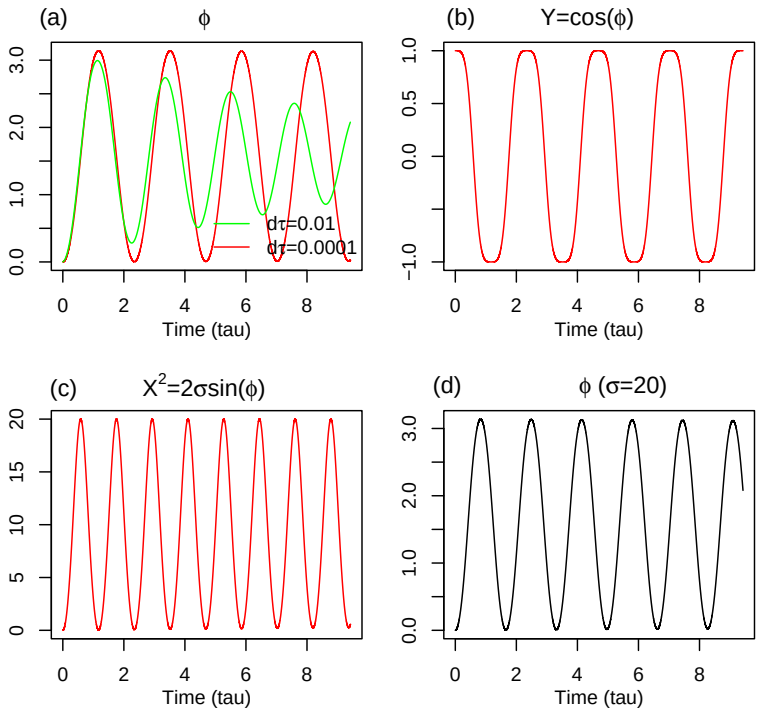

Fig. 2. Solutions of Eq. (24a) and (24b) with the iterated method. **(a)** The phase function (ϕ) with $\Delta\tau = 0.01$ (green) $\Delta\tau = 0.0001$ (red) (Eq. 24b), **(b)** $Y = \cos(\phi)$ (Eq. 22b) and **(c)** $X^2 = 2\sigma\sin(\phi)$. (Eq. 22a). **(d)** The phase function with a different value of σ (= 20).

NPGD
1, 519–541, 2014

A 3D-NLM

B.-W. Shen

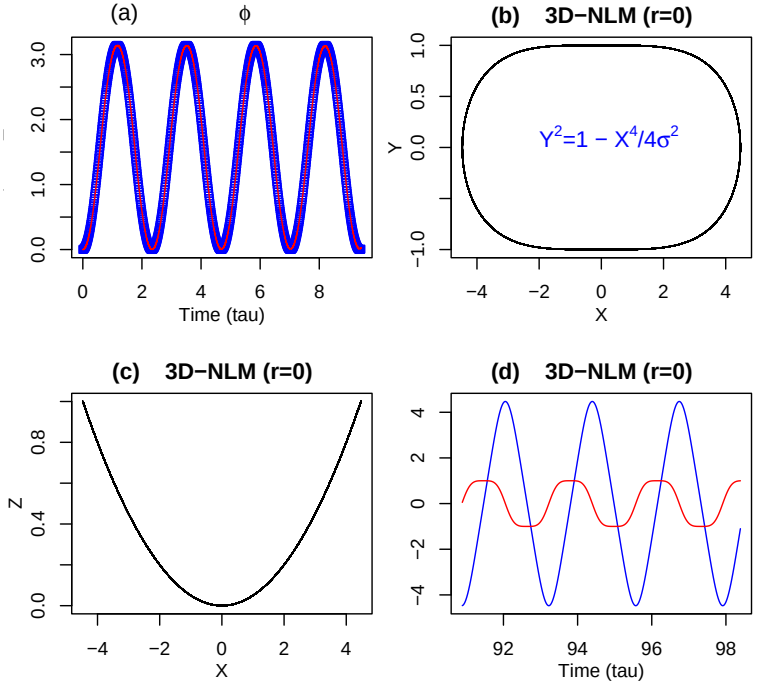

Fig. 3. Solutions from the 3D-NLM (Eqs. 3–5) with $r = 0$. **(a)** A comparison of the phase functions, which are calculated from the 3D-NLM (blue dot) and Eq. (24a) and (24b) (red). **(b)** X–Y plot. **(c)** X–Z plot. **(d)** Time evolution of X (blue) and Y (red).

NPGD
1, 519–541, 2014

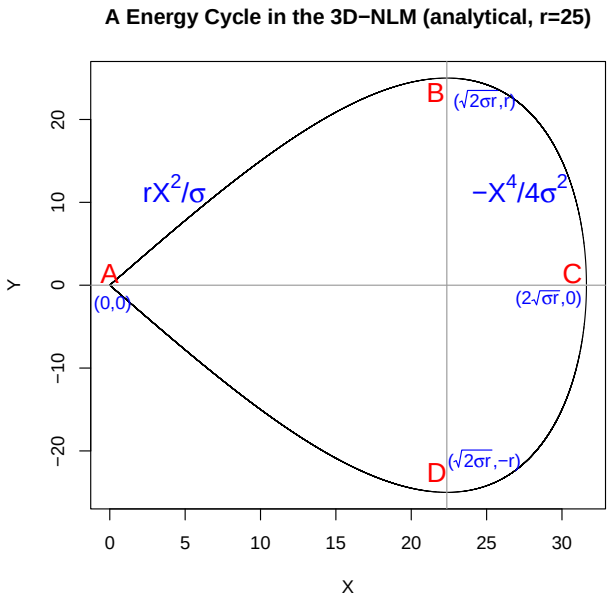

Fig. 4. An energy cycle in the 3-D non-dissipative Lorenz model (3D-NLM) as shown in the X–Y plot. The four points with the selected ICs are identified as follows: $A(X,Y) = (0,0)$, $B = (\sqrt{2\sigma r}, r)$, $C = (2\sqrt{\sigma r}, 0)$, and $D = (\sqrt{2\sigma r}, -r)$. $(\sigma, r) = (10, 25)$. The energy cycle starts at (near) point A, $A^+ = (0, 0^+)$ to be specific, goes through B, C, and D, and returns back close to A, i.e., $A^- = (0, 0^-)$. KE increases as APE decreases along the upper curve (Legs A–B and B–C) and KE decreases as APE increases along the lower curve (Legs C–D and D–A). From a perspective of potential energy partition, $\|\mathrm{APE}_Y\| \geq \|\mathrm{APE}_Z\|$ in Legs A–B and D–A where linear force dominates, and $\|\mathrm{APE}_Y\| \leq \|\mathrm{APE}_Z\|$ in Legs B–C and C–D where nonlinear restoring force dominates.

NPGD
1, 519–541, 2014

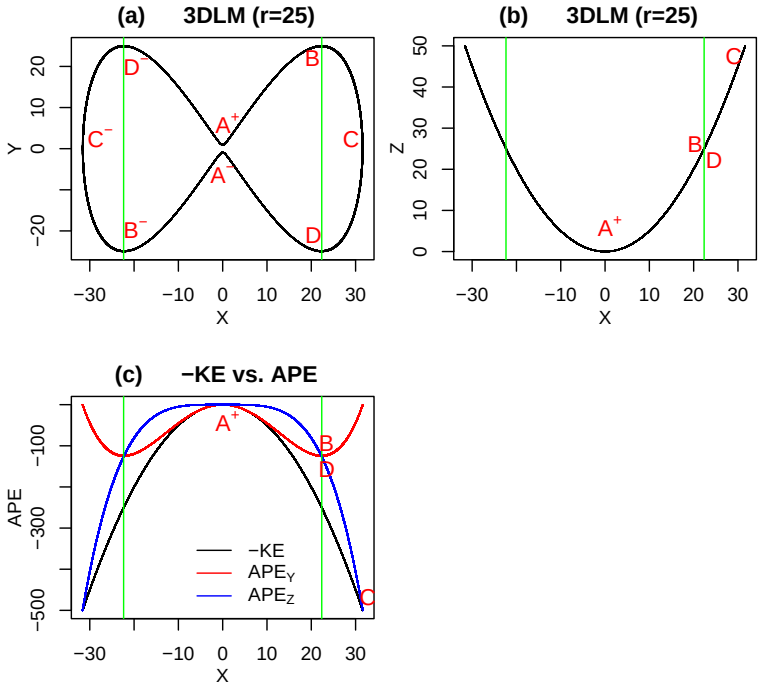

Fig. 5. Solutions from the 3D-NLM (Eqs. 3–5). **(a)** X–Y plot. **(b)** X–Z plot. **(c)** X-APE plot. The black, red, blue lines show normalized −KE, APE$_Y$ and APE$_Z$, respectively. Green lines are plotted at $X = \pm X_t = \pm\sqrt{2\sigma r}$ where $Y^2 = Z^2$.

NPGD
1, 519–541, 2014

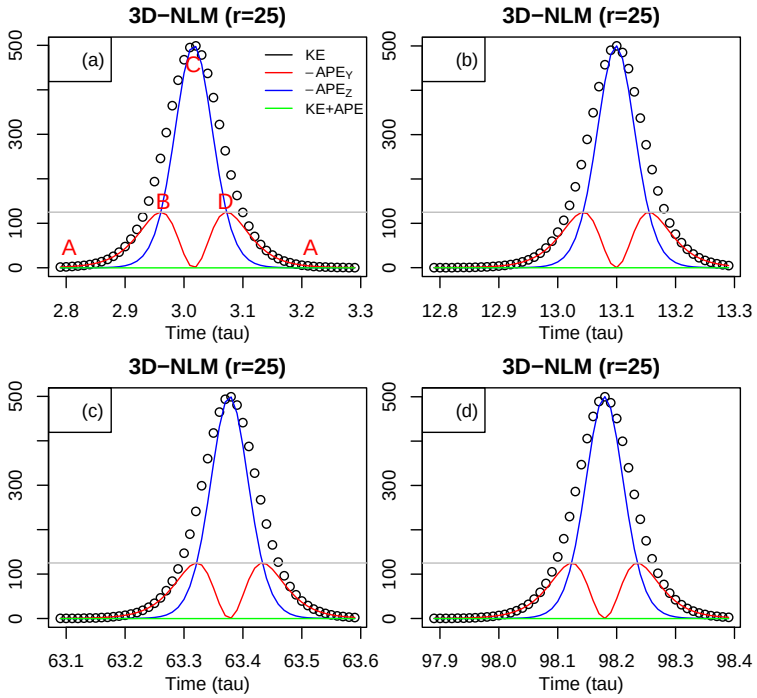

Fig. 6. Time evolution of the KE and APE in the 3D-NLM (Eqs. 13 and 14). While the black open circles display KE, the red, blue and green lines show $-\mathrm{APE}_Y$, $-\mathrm{APE}_Z$ and $\mathrm{KE}+\mathrm{APE}$, respectively. All of the fields are normalized by C_o. The gray line is plotted at a value of $\sigma r/2$, which is equal to $-\mathrm{APE}_Y/C_o$ and $-\mathrm{APE}_Z/C_o$ at $X = X_\mathrm{t}$. These panels show that solutions are oscillatory and periodic.

NPGD
1, 519–541, 2014